RAIN RATE-REFLECTIVITY RELATIONSHIP FOR MARINE STRATUS

by
Qing Yang

A thesis submitted to the Department of Atmospheric Science
and The Graduate School of The University of Wyoming
in partial fulfillment of the requirements
for the degree of

MASTER OF SCIENCE
in
ATMOSPHERIC SCIENCE

Laramie, Wyoming
December, 2002

TABLE OF CONTENTS

LIST OF FIGURES

LIST OF TABLES

ACKNOWLEDGMENTS

1. Introduction

Accurate measurement of rainfall is of great importance from many perspectives, including hydrology and cloud physics. In cloud physics, estimation of the water budget of clouds (precipitation efficiency) remains a major problem. Rainfall intensity is known to have high spatial variability, yet common measurements of rainfall rely on instruments which provide point measurements only. Hence, the standard measurements are inadequate for providing accurate and detailed area rainfall information.

Meteorological radars detect rain (or other forms of precipitation) and readily yield area (or volume) measurements, but radar reflectivity is not equal to rain rate. The power intercepted by the radar antenna $\overline{P_r}$ is proportional to "reflectivity" which is the integral of the backscatter cross sections, σ, of the hydrometers per unit volume of air. Assuming Rayleigh scattering at wavelength λ, the reflectivity is given by

$$\eta = \int_{vol} \sigma_i d\sigma_i = \frac{\pi^5}{\lambda^4} |K|^2 \int_0^{D_{max}} N(D)dD \qquad \text{--------- (1)}$$

where K is the absorption coefficient of the material involved (water or ice), D is the spherical particle diameter, and N(D) is the size distribution. Radar reflectivity factor Z is proportional to the sixth moment of the droplet size distribution (DSD),

$$Z = \int_0^{D_{max}} D^6 N(D)dD, \qquad \text{--------- (2)}$$

so that
$$\eta = \frac{\pi^5}{\lambda^4} |K|^2 Z. \qquad \text{--------- (3)}$$

Thus, if it is known that all the scatterers are either liquid or solid so that K is a constant, the radar reflectivity is proportional to the reflectivity factor, which is dependent only on the DSD.

Rain rate (R) is roughly proportional to fourth or fifth moment of the DSD:

$$R = 6\pi \cdot 10^{-4} \int_0^{D_{max}} D^3 v(D) N(D) dD \qquad \text{---------- (4)}$$

where $v(D)$ (m s^{-1}) is the terminal velocity of raindrops which varies as D^2 for small droplets and as D^1 for larger ones, and D is the spherical particle diameter (Gunn and Kinzer, 1949). All of the foregoing are valid for drop sizes smaller than the wavelength (D<0.1λ). In this study, Mie correction was applied to drop sizes bigger than 100μm. The Mie correction factor is close to 1 and the maximum Mie correction is about 10%.

Without information about the drop spectra, it is difficult to predict a direct relationship between Z and R. Several approaches have been implemented to predict empirical Z-R relationships: (i) R and Z calculated from assumed or measured drop spectra; (ii) comparison of rain gauge and radar measurements; and, (iii) measurement of Z converted via an assumed Z-R relationship to predict R, then comparing the predicted R with measured R. In this study, the first approach is employed.

Most studies have yielded empirical relationships of the form $Z = a R^b$, where a and b are constants. However, a and b have been found to vary widely with rainfall types and locations. Battan (1973) presents numerous Z-R relationships found for different types of rain and different locations. Some examples are given in Table 1.

Early Z-R expressions were obtained by measuring raindrop spectra. Rainfall intensity was either calculated from the raindrop data or observed directly. Radar reflectivity factor Z was obtained by computation. Caton (1964) measured R by means of a rain gauge at the same time that a vertical pointing 3-cm pulsed-Doppler radar set was used to determine raindrop spectra. This work yielded Z [mm^6 m^{-3}] = 240 R$^{1.30}$ [mm h^{-1}].

Table 1: Empirical Relationships between Reflectivity Factor, Z ($mm^6\,m^{-3}$), and Rate Rate, R ($mm\ h^{-1}$)

Equation	Reference	Location	Remarks
$Z = 320R^{1.44}$	Wexler, R. (1947)	Washington D.C.	Storms (8 rain intensities)
$Z = 16.6R^{1.55}$	Blanchard (1953)	Hawaii	Orographic rain
$Z = 486R^{1.37}$	Jones (1955)	Central Illinois	thunderstorms
$Z = 162R^{1.16}$	Atlas and Chmela (1957)	Lexington, Mass	Stratiform rain
$Z = 350R^{1.42}$	Atlas and Chmela (1957)	Lexington, Mass	Stratiform rain
$Z = 66.5R^{1.92}$	Sivaramarkri	Poona, India	Warm rain
$Z = 300R^{1.37}$	Fujiwara	Mostly Miami, Florida	rainshowers
$Z = 205R^{1.48}$	Fujiwara	Mostly Miami, Florida	Continuous rain
$Z = 426\ R^{1.5}$	Cogombles (1966)	France	107 DSD

Seliga et al (1986) used a disdrometer in a highly variable, heavy rainfall event in central Illinois and deduce the relationship, $Z\ [mm^6\,m^{-3}] = 388\ R^{1.36}\ [mm\ h^{-1}]$. The study showed this equation gave an excellent agreement between the disdrometer and radar derived rainfall. In 1996, the National Center for Atmospheric Research (NCAR) carried out a program in radar hydrology to improve Z-R relationship technology for estimating precipitation. In this program, radar reflectivity-based rainfall estimates from collocated radars were computed with the WSR-88D default relationship $Z = 300.8\ R^{1.4}$. The correlation coefficient between gauge observations and radar estimates varied from 0.78 to 0.90. (Brandes et al, 1999). This investigation consisted of convective storms, most of which were attended by stratiform rain areas, and it showed large storm to storm variations in mean bias (defined as the ratio of gauge and radar amounts), a primary source of storm to storm bias lied with variation in drop size distributions and

consequently, variations in the relationship between radar reflectivity and rainfall rate (Brandes et al, 1999).

As these examples illustrate, it is important to find Z-R relationship appropriate for each type of precipitation. Thus, a specific study of the Z-R relationships for stratus clouds is essential to produce a Z-R relationship applicable for stratus clouds.

Stratus clouds are important in boundary layer dynamics and global climate (Frisch et al, 1998). Stratus and stratocumulus clouds form in shallow layers (~1 km or less in vertical extent), with low liquid water content (mostly less than 1 g kg^{-1}), and small vertical motion (about 10-100 cm s^{-1}) (Houze, 1993). Nevertheless, stratus and stratocumulus clouds have high albedos and reduce the short wave radiation received at the earth's surface. They are observed to occur in persistent sheets covering large areas of the eastern parts of subtropical oceans, as more transient features under mid-latitude anticyclones, and in arctic regions (Martin, 1994). Marine stratus play an important role in the earth radiation budget (Nicholls, 1984), and they may be an important factor in global climate change. Randall (1984) has shown that a 4% increase in the area covered by stratocumulus would result in atmospheric cooling that could offset global warming due to doubling the CO_2 content of the atmosphere. Full understanding of the properties of these clouds will be vital for estimating global energy budgets and to set up numerical weather and climate model simulation realistically.

In this work, Z-R relationships were derived for coastal/marine stratus clouds, using data from the "Coastal Stratus 1999" (CS99) and from the "Dynamics and Chemistry of Marine Stratocumulus" (DYCOMS) projects. Airborne particle probes and other airborne instruments installed on research aircraft offered in situ and more accurate

measurements of DSD and other properties of the clouds. R and Z are calculated from size distributions measured by aircraft instruments. The relationships so obtained provide a basis for deriving drizzle rate* in marine stratus from airborne radar measurement. Drizzle rate (R) in this study refers to the vertical flux of hydrometeors relative to air, rather than relative to the ground as most commonly used for precipitation rates.

2. Methodology

The data for this study are from two field research projects, CS99 and DYCOMS-II. CS99 was a study of coastal stratus off the Oregon coast utilizing the Wyoming King Air research aircraft, during August 5 to September 4, 1999. DYCOMS-II was carried out west-southwest of San Diego California using the NCAR/ C130 aircraft during July 7 to July 28, 2001.

Flights for both projects include multiple horizontal legs at varying altitude levels. Seven out of nine research flights of DYCOMS-II were nocturnal and flights of DYCOMS-II covered areas further away from coast than the flights of CS99.

Both research aircraft were equipped with instruments to measure hydrometeor size distributions, radiation, cloud liquid water content, thermodynamic and state parameters, position, attitude, relative air motion and so on. The instruments used to obtain the hydrometeor measurements were PMS (Particle Measuring Systems, Inc, Boulder, Co) probes: the forward scattering spectrometer probes (FSSP100), the 1D-C optical array probes (200X for CS99 and 260X for DYCOMS-II), and the 2D-C optical array probes.

Since stratus yields low rainfall rate, it is usually referred to as drizzle. For generality, the term 'rain rate' in used here even when describing drizzle.

During the CS99 project, the FSSP100 collected data in 15 size categories with a measurement range of 0.5-47.5 μm. The data for our study were recorded with bin sizes of 3 μm at 1Hz. For DYCOMS-II, FSSP100 measurements were categorized into 41 bins of equal sizes with a range of 1 to 47 μm. The data for our study were recorded with bin sizes of 1.152 μm at 1Hz. With these probes, the sizes of the sampled hydrometors were determined by measuring the light scattering intensity, and using Mie scattering theory to relate measured intensity to particle size. Monodispersed polystyrene and glass beads were used for the calibration of the FSSP. For CS99, the estimated accuracy of total droplet concentrations is about 10%, with sizing accuracy around 15%. For DYCOMS-II, the estimated accuracy of total droplet concentrations is 16%, with sizing accuracy of 20% (http://atd.ucar.edu/dir_off/airborne/index.html).

The 200X (1D-C) optical array probe used in CS99 measures particle sizes ranging from 12.5 to 185.5 μm in 15 channels. For DYCOMS-II, the 260X probe has a measurement range of 15 to 645 μm in 64 channels. In these probes, when a hydrometeor passes through a focused He-Ne laser beam, the number of photodiodes occulted during its passage determines its size. Particles that shadow either one of the end photodiodes are rejected so that only particles that pass entirely within the boundary of the array are counted. Monodispersed beads were used for the calibration.

The 2D-C optical array probe has a resolution of 25μm for both projects. For CS99, the 2D-C data were categorized into 20 intervals with bin sizes of 50 or 100 μm for particles less than 1000 μm. For DYCOMS-II, the 2D-C has a measurement range of 17-1592 μm in 64 size categories of 25 μm increments. For CS99, sizes represent the

maximum dimensions along the flight direction; this treatment leads to a possible underestimation of drop size by about 25μm due to the electronic delay in triggering the detector circuits (Vali et al, 1998). For DYCOMS-II, information about a particle's size was deduced from reconstruction of the recorded shadow with "Center-in" approach.
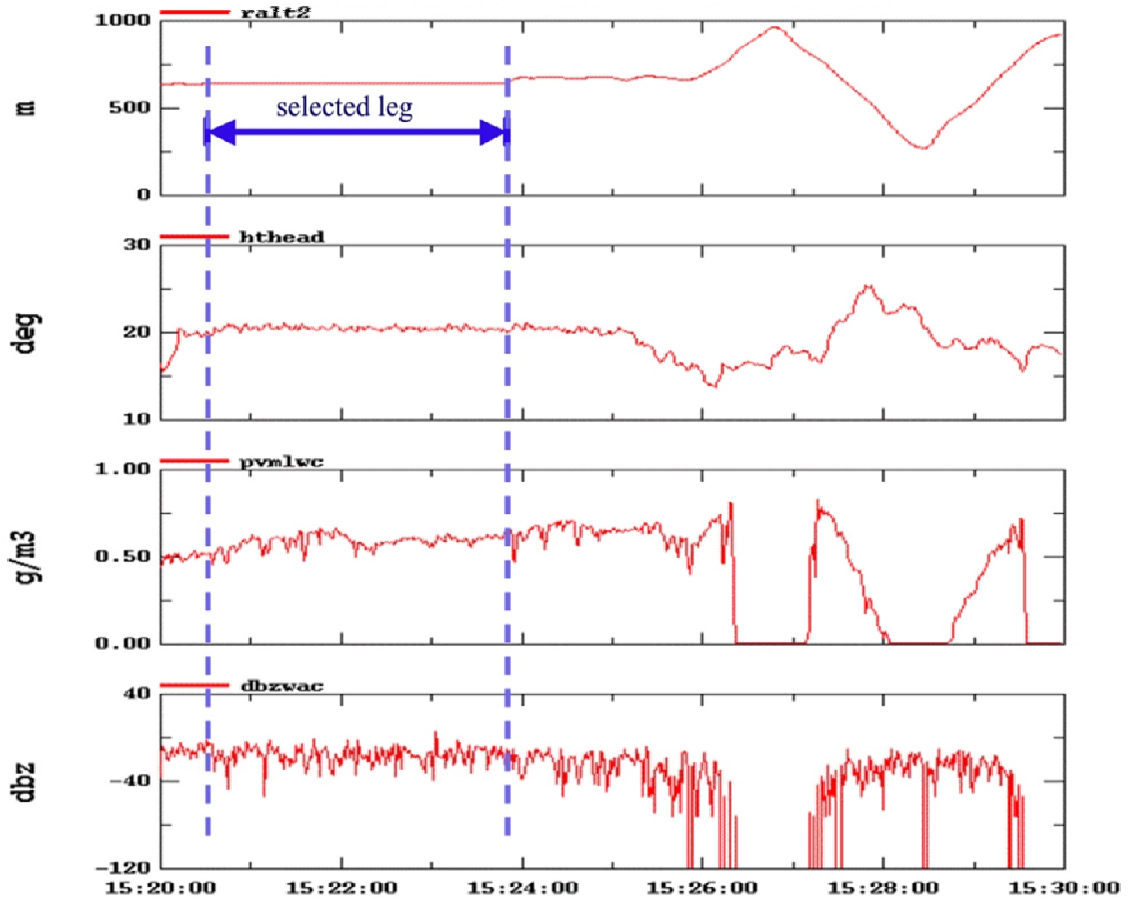
Figure 1: Example of flight segments selection (CS99, 081799, 15:20:00-15:30:00). *ralt2* is an altitude parameter, *hthead* is a heading parameter, *pvmlw*c is the liquid water content from PVM probe, *dbzwac* is the derived radar reflectivity.

From both projects, level flight segments (legs) longer than 120 seconds and that were continuously in cloud or in precipitation were chosen by using the following criteria: liquid water content exceeds 0.05g m^{-3} or the derived radar reflectivity exceeds

−40 dbz, and the flight heading and flight altitude are constant. Choosing data with constant heading and altitude avoids the influence of flight maneuvers. Data records of 1Hz resolution were used. Figure 1 demonstrates an example of how the flight segments were chosen using the above criteria.

After the selection of flight segments, data were screened using the following criteria: for each second, relative error, that is mean standard deviation of counts divided by total counts, should be less than 15% for CS99, and FSSP concentrations should exceed 25 counts per second for DYCOMS-II. Data that did not pass the screening were discarded.
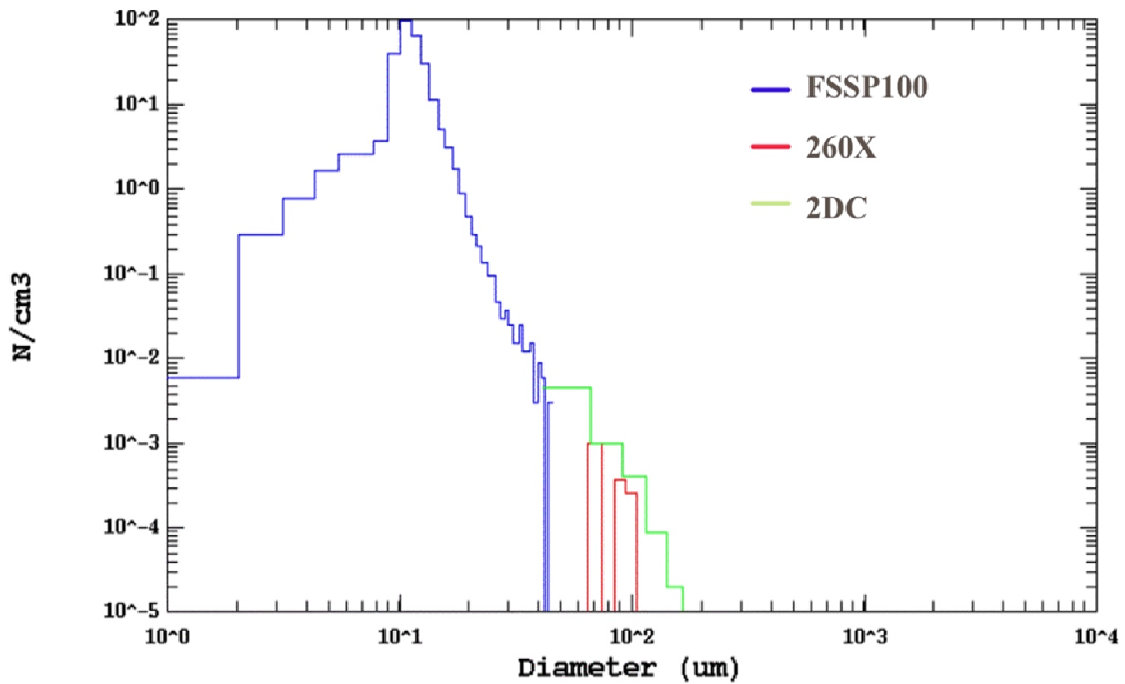
Figure 2: An observed spectrum from 3 probes (DYCOMS-II, 071301, 10:21:47-10:21:57, 10 second average).

If it is assumed that droplets are randomly distributed in space, and that the average rate at which particles are sampled is constant over a given interval of time, then the Poisson distribution is valid for our data. Since the relative error for Poisson statistics is $\sqrt{N}/N$, where N is the total counts per second from three probes, in order to pass the screening test, total counts per second from three probes should exceed 45 for CS99. That is:

$$N = \Sigma \text{ (sample volume per second)*(number conc)} > 45 \text{ s}^{-1}.$$

In all selected flight segments, rain rate and reflectivity were calculated for each second that passed the screening test, using DSD constructed from measurements from the three PMS probes. In the constructed DSD for CS99, FSSP data were used for droplet diameters D ≤ 47.5μm; 1-D data were used for 47.5μm < D ≤ 100μm; and 2-D data were used for 100μm < D ≤ 1000μm. For DYCOMS-II, only FSSP and 2-D data were used for the construction of the spectra, with the separation at 50μm. The reason for not using the 1-D data of DYCOMS-II for the construction of DSD can be explained using Figure 2: In typical spectra, apparently, when compared to the 2D probe, the 260X probe was grossly under sampling.

For all selected legs, rain rate and reflectivity were calculated for each second using equations 2 and 4, respectively. In equation 4, for droplets with D ≤ 60 μm, the droplet terminal velocity was estimated from Stokes' Law, which has a quadratic dependence of fall speed on size:

$$\upsilon(D) = k_1 \left(\frac{D}{2}\right)^2 \qquad \text{--------- (5)}$$

with $k_1 \approx 1.19 \times 10^6$ cm^{-1} s^{-1}. For 60µm < D $\leq$ 1000µm, linear dependence of velocity on size was employed for the estimation of terminal velocity:

$$\upsilon(D) = k_2 \left(\frac{D}{2} \right)$$ -------- (6)

with $k_2 \approx 8 \times 10^3$ s^{-1} (Rogers and Yau ,1989).
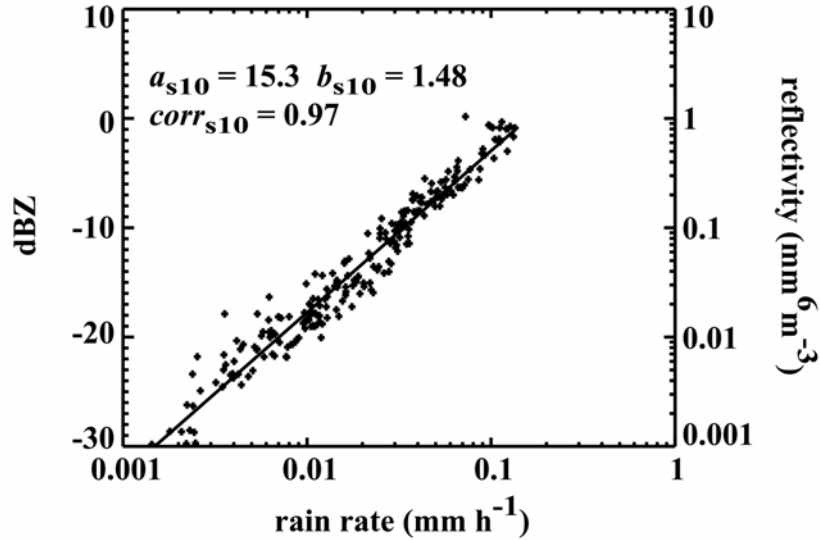
Figure 3: Rain rate vs. reflectivity for leg #10 (CS99, 081199, 15:50:42-15:55:45). The leg length is 303 seconds. The a_{s10} & b_{s10} are parameters in $Z = a\, R^{\,b}$, and the $corr_{s10}$ is the correlation coefficient of log(Z) & log(R). The straight line is the best-fit line for log(Z) vs. log(R).

In order to avoid the influence of a few data that scatter far away from the data group at low and high ends of the range, only 5-95 percentile of the calculated rain rate and reflectivity for each second were used. Along with a correlation coefficient, the a and b parameters in empirical relationships of the form $Z = a\, R^{\,b}$ were calculated for each leg and for all data combined per day, using a least-square fit for log(Z) = a + b log(R). An example is shown in Figure 3. Note that the least-square fits apply to log(Z), but the data and the fitted line are plotted as dBZ (10 log(Z)).

Since the observed data sets have fewer data at the high value and low value ends, to give equal emphasis to data in different range area, symbolic data points with 1dBZ interval in Z were produced by implementing the obtained Z-R relationship for each leg within their ranges of validity. Newly produced symbolic data sets were used to generate Z-R relationships for the whole projects.

To explore the impact that potential under-detection of larger droplets would have on the Z-R relationships, droplet spectra were extrapolated to droplet sizes of 500μm and 1000μm based on a best-fit line for droplets larger than 30μm in diameter. In addition, the fit was further refined using average spectra with 5, 10, and 15 seconds intervals, and with 500μm and 1000μm upper size limits for the analytic expression that replaces the observed data.

Confidence limits of the generated Z-R relationships were determined. Error bars for each size bin of one-second spectra were estimated based on Poisson statistics. The spectra defined by the upper and lower limits of the error bars construct two spectra that bracket the original data. By comparing rain rate and reflectivity calculated from the newly constructed spectra according to error bars and the original spectrum, and following the same methodology used to generate the Z-R relationships, the confidence limits of the Z-R equations was determined.

Further, the dependence of the Z-R relationships on normalized cloud depth and on mean droplet concentration was studied for both projects.

3. Results

3.1 Short Flight Segments

For the CS99 and DYCOMS-II projects, 12485 and 23668 seconds of data were processed, respectively, for this study. A total of 60 flight segments (leg No = si, i = 1-60) were selected for CS99; the length of these legs varied from 120 seconds to 744 seconds with an average of 250 seconds. DYCOMS-II had 75 flight segments (leg No = si, i = 61-135) with a leg length of about 300 seconds. For each leg, the Z-R relationship was obtained by calculating the a and b parameters according to the equation $Z = a\,R^{b}$.
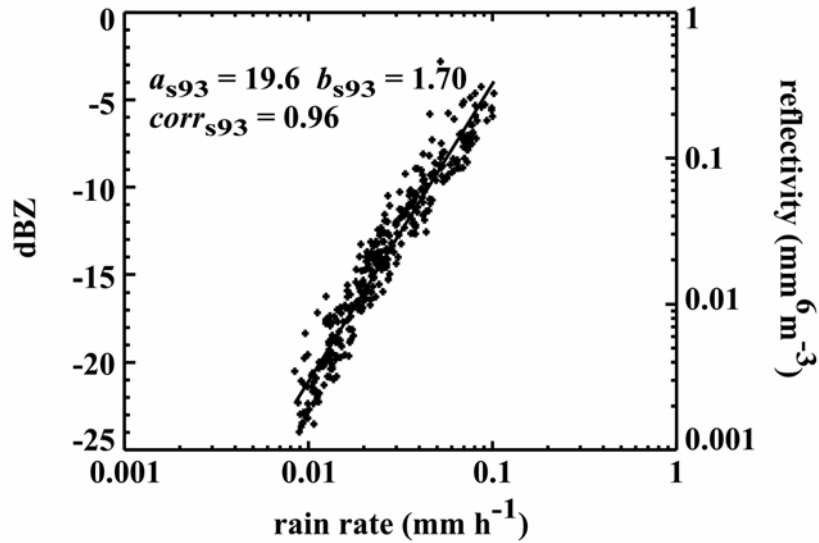
Figure 4: Rain rate vs. reflectivity for leg # 93 (DYCOMS-II, 072401, 09:08:44-09:13:43). The leg length is 300 seconds. The a_{s93} & b_{s93} are parameters in $Z = a\,R^{b}$, and the $corr_{s93}$ is the correlation coefficient of log(Z) and log(R). The straight line is the best-fit line for log(Z) vs. log(R).

Figures 3 and 4 show examples of the Z-R scatter plots for one leg of CS99 and for one leg of DYCOMS-II, respectively. The correlation coefficients for individual legs of CS99 range from 0.82 to 1.0 with an average of 0.96. For DYCOMS-II, the correlation coefficients vary from 0.85 to 1.0 with an average of 0.93. In Figures 5 and 6, the histograms of a and b demonstrate the variation of Z-R relationships among flight segments. The plotted values include only the 5 - 95 and 10 - 90 percentiles of the Z-R
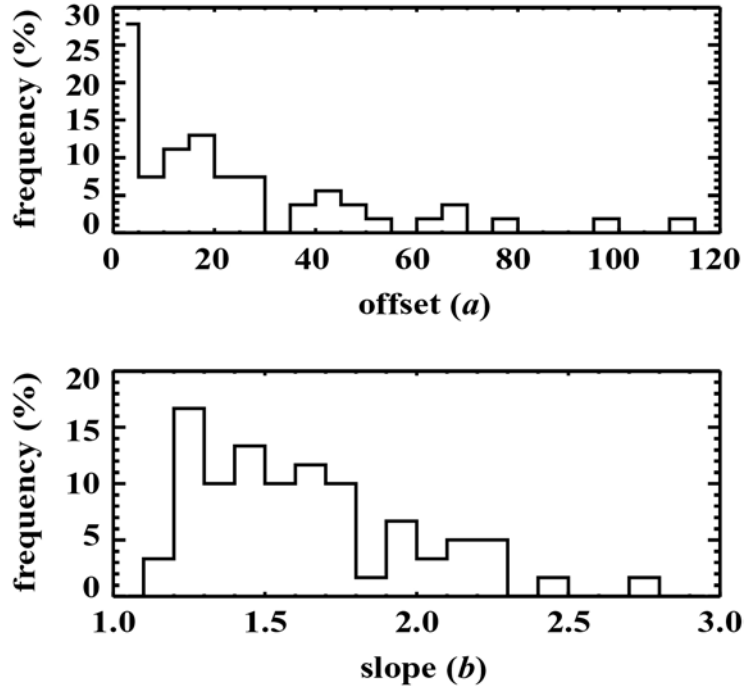
Figure 5: Histograms of Z-R parameters for CS99 (5-95 percentile of the *a* & *b* parameters for total 60 flight segments).
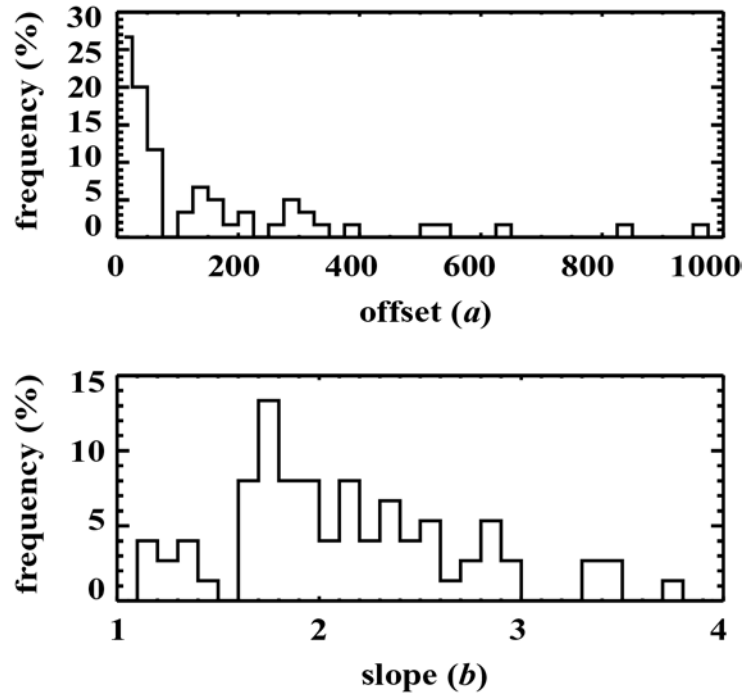
Figure 6: Histograms of Z-R parameters of DYCOMS-II (5-95 percentile of the *a* & *b* parameters for total 75 flight segments)
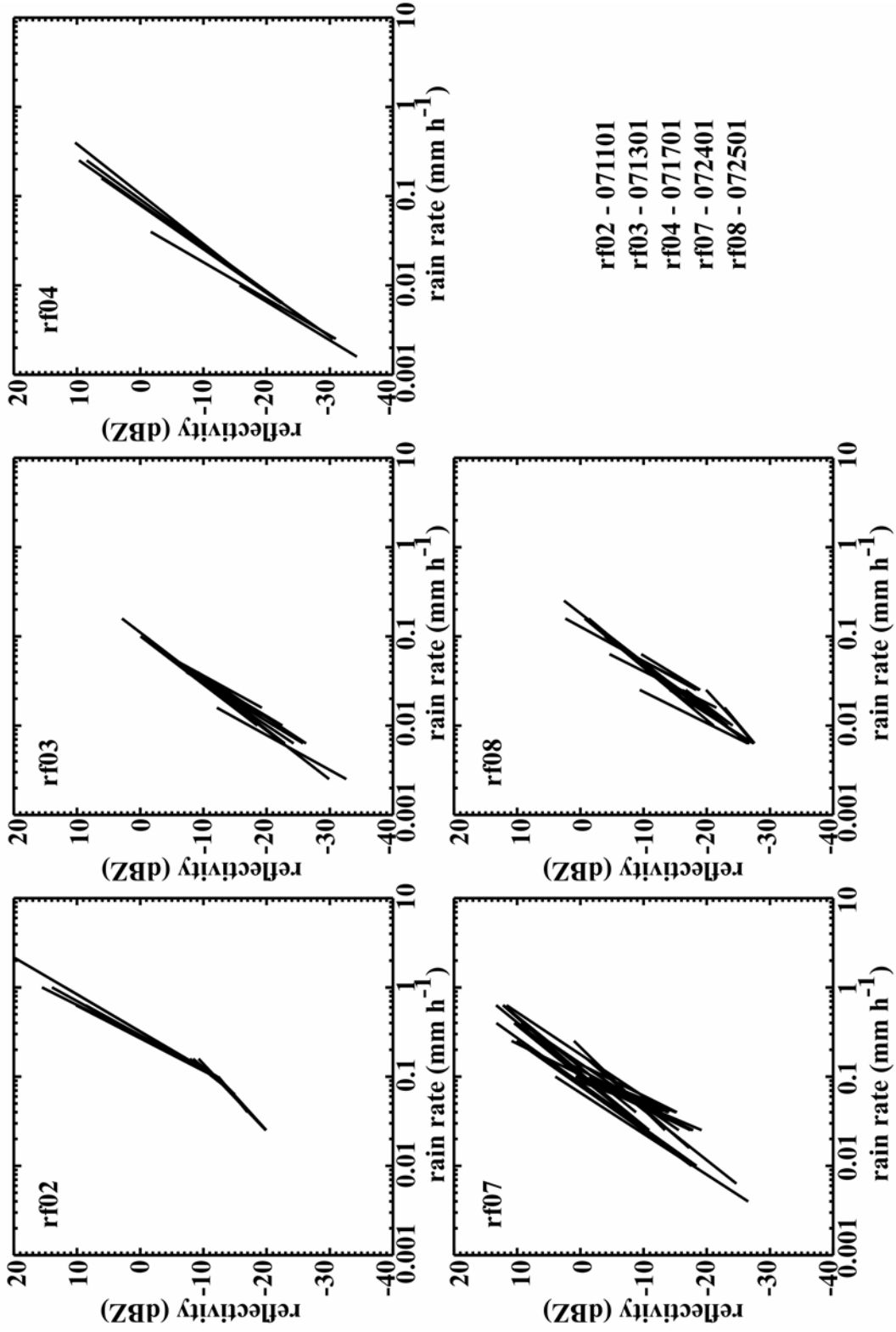
Figure 7: Rain rate *vs.* reflectivity best-fit lines within their ranges of validity by day (DYCOMS-II)

parameters for CS99 and DYCOMS-II, respectively. Some extreme values occurred due to inhomogeneous samples. For CS99, the offset parameter a_{si} (i = 1-60) varies from 1.2 to 115, with about 28% of the values less than 5; the slope parameter b_{si} (i = 1- 60) varies from 1.1 to 2.8, with about 17% of the values between 1.2 and 1.3 and about 73% between 1.2 and 1.8. Compared to CS99, DYCOMS-II demonstrates larger variability in both offset and slope parameters. The offset a_{si} (i = 61-135) in Figure 6 varies from 1.4 to around 1000, with 26% of the values less than 25 and about 58% less than 75; the slope b_{si} (i = 61-135) range from 1.1 to 3.8 with 13% falling between 1.6 and 1.7 and 37% between 1.6 and 2.0. The lists of the Z-R parameters for all short flight segments are attached as Appendix A and Appendix B.

Another way to examine the degree of variability, the best-fit lines for each leg within their ranges of validity are shown in Figure 7 for each day of the DYCOMS-II project. Except for one day (rf02), the lines group together quite well, indicating good uniformity of cloud composition.

3.2 Aggregate data by day

Data were combined to generate a Z-R relationship for each flight day as shown in Figures 8 and 9. The Z-R parameters so obtained for each day are tabulated in Tables 2 and 3. For CS99 project, the daily values of a_{dj} (j = 1-8) vary from 0.8 to 41.1 and from 1.14 to 2.01 for b_{dj} (j = 1-8). For DYCOMS-II, the day-to-day variation is 2.5 to 166.8 for a_{dj} (j = 9-14) , and 1.37 to 2.01 for b_{dj} (j = 9-14).
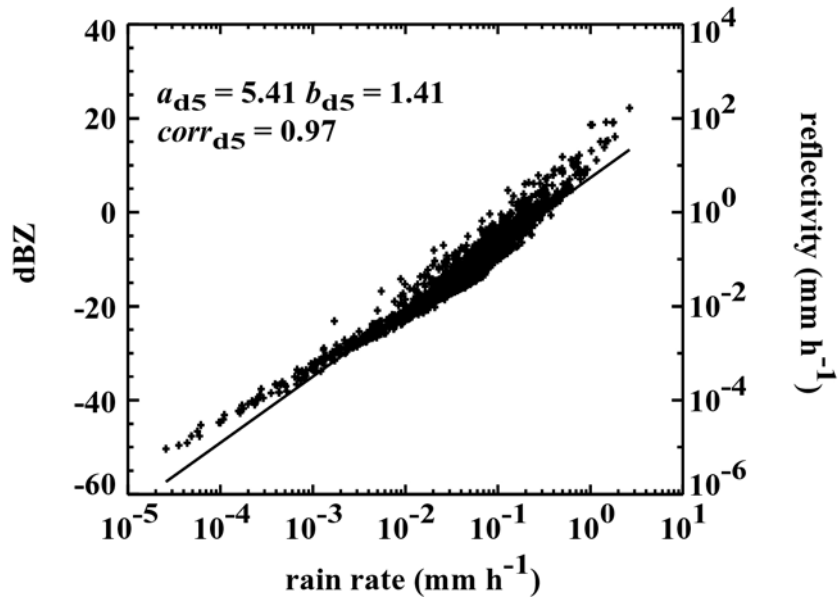
Figure 8: Rain rate vs. reflectivity for day #5 (CS99, 082099). Number of data points is 1630. The a_{d5} & b_{d5} are parameters in $Z = a R^{\,b}$, and the $corr_{d5}$ is correlation coefficient for log(Z) vs. log(R). The straight line is the best-fit line for log(Z) & log(R).
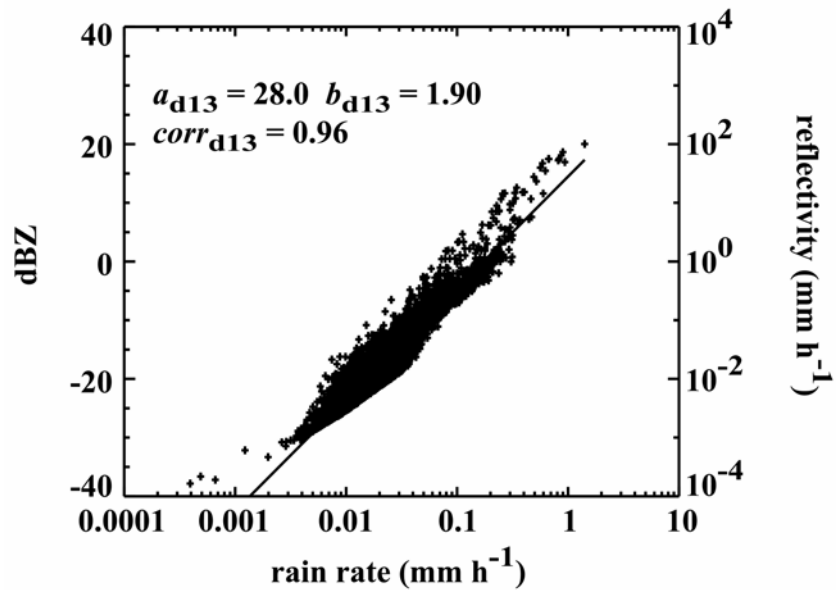
Figure 9: Rain rate vs. reflectivity for day #13 (DYCOMS-II, 072501). Number of data points is 5570. The a_{d13} & b_{d13} are parameters in $Z = a R^{\,b}$, and the $corr_{d13}$ is correlation coefficient for log(Z) vs. log(R). The straight line is the best-fit line for log(Z) & log(R).

Table 2: Z-R parameters for each flight day of CS99

day No.(j)	date	a_{dj}	b_{dj}	c_{dj}	ptn
1	080999	1.70	1.14	0.95	1675
2	081199	6.55	1.40	0.94	2540
3	081699	2.29	1.28	0.93	2060
4	081799	41.1	2.01	0.95	1430
5	082099	5.41	1.41	0.97	1630
6	082199	1.14	1.20	1.00	579
7	082499	0.832	1.18	0.96	1210
8	082899	5.68	1.58	0.92	1361

a_{dj} & b_{dj} are constants in $Z = a R^b$; c_{dj} is the correlation coefficient for log(Z) vs. log(R); *ptn* is the total data points for one day.

Table 3: Z-R parameters for each flight day of DYCOMS-II

day No.(j)	date	a_{dj}	b_{dj}	c_{dj}	ptn
9	071101	2.50	1.37	0.94	3519
10	071301	21.8	1.64	0.90	3793
11	071701	166	2.01	0.98	1798
12	072401	52.9	1.96	0.91	6817
13	072501	28.0	1.90	0.96	5570
14	072701	10.0	1.59	0.94	2171

a_{dj} & b_{dj} are constants in $Z = a R^b$; c_{dj} is the correlation coefficient for log(Z) vs. log(R); *ptn* is the total data points for one day.
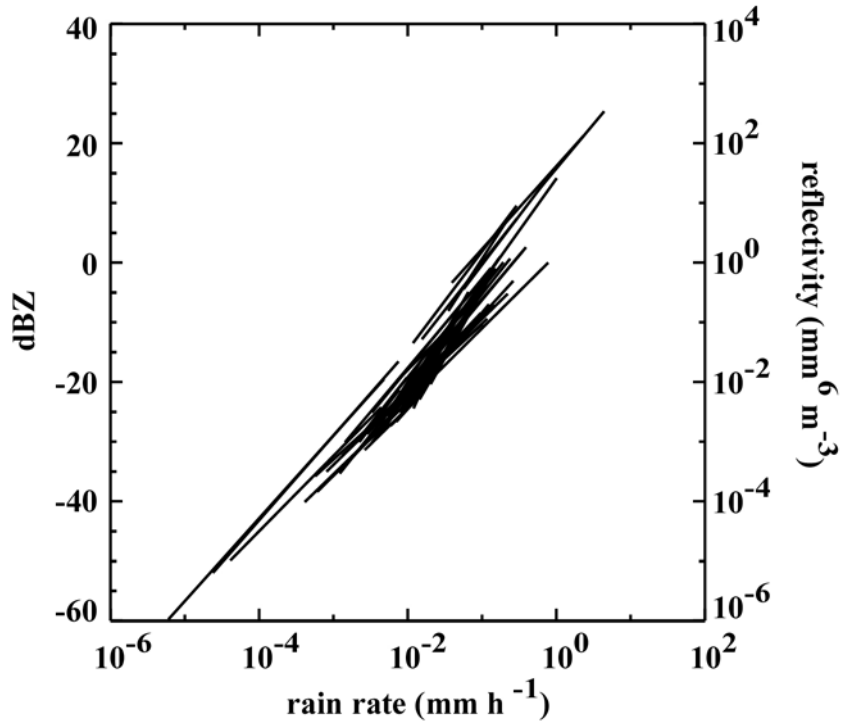
Figure10: Z-R relationships for individual legs of CS99
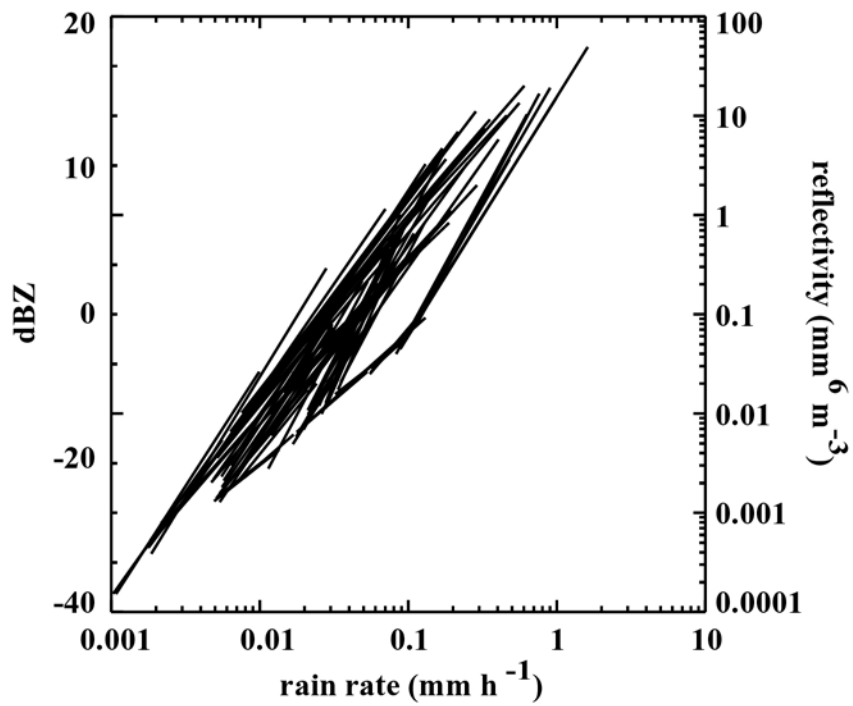
Figure 11: Z-R relationships for individual legs of DYCOMS-II
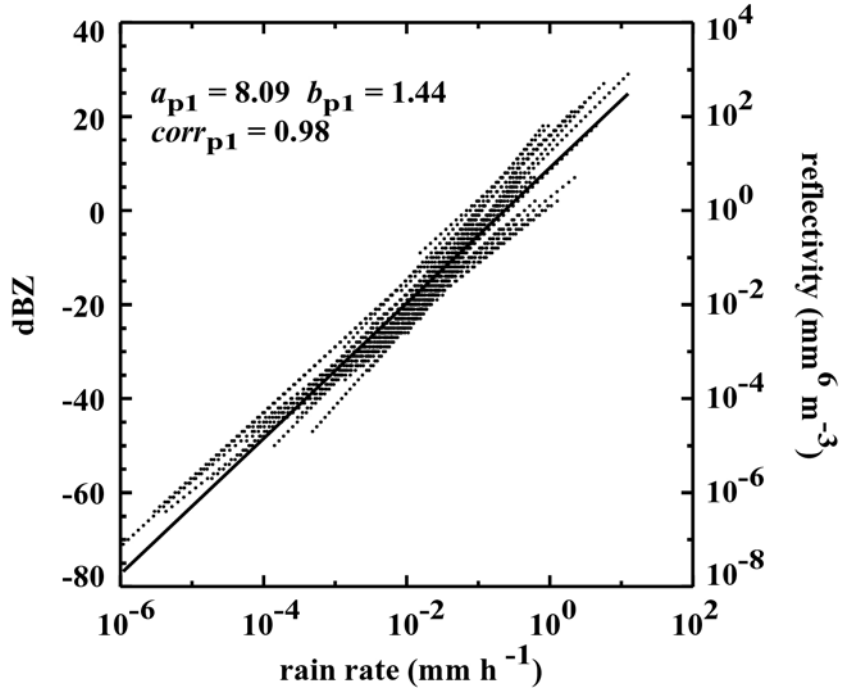
Figure 12: Rain rate vs. reflectivity for synthetic data of CS99. The a_{p1} & b_{p1} are parameters in $Z = a R^{b}$, and the $corr_{p1}$ is correlation coefficient for log(Z) vs. log(R). The straight line is the best-fit line for log(Z) & log(R).
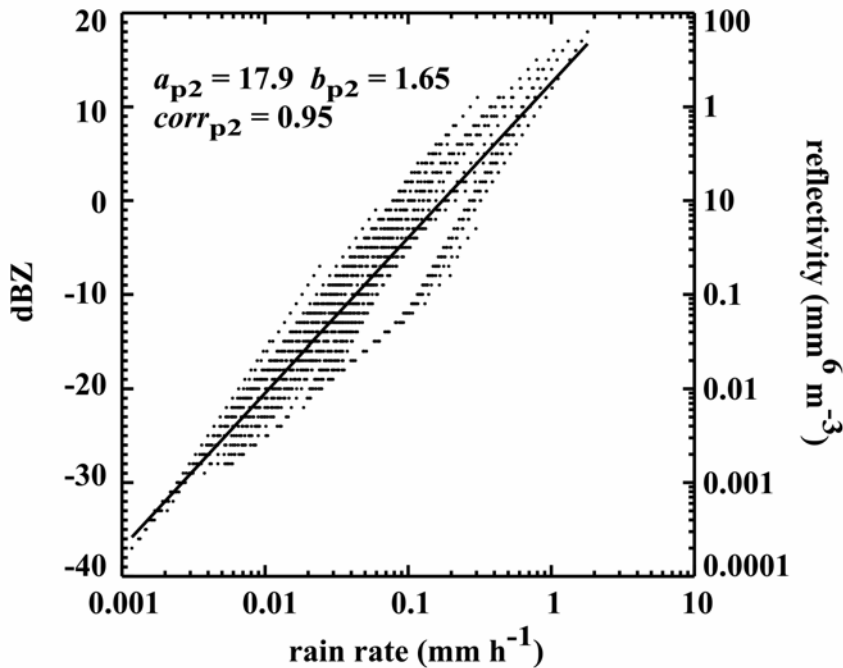
Figure 13: Rain rate vs. reflectivity for synthetic data of DYCOMS-II. The a_{p2} & b_{p2} are parameters in $Z = a R^{b}$, and the $corr_{p2}$ is correlation coefficient for log(Z) vs. log(R). The straight line is the best-fit line for log(Z) & log(R).

3.3 Aggregate data by project

The Z-R equations for individual flight segments are plotted in Figures 10 and 11 for CS99 and DYCOMS-II. To combine all the data by project, the following procedure was adopted. Since there are fewer observations at the high and low ends of the ranges of R and Z, and because it is desirable to have the Z-R equation give the best possible estimate over as large a range of values as the data justifies, the large numbers or redundant points at mid-range were de-emphasized. Therefore, the Z-R relationships for individual flight segments were used to obtain pairs of Z and R data points at Z intervals of 1dBZ within the range of validity of each individual flight segment. The newly generated synthetic data points from all flight segments were used to calculate a best-fit Z-R relationship for the whole project. Figures 12 and 13 show the synthetic data and the resulting Z-R relationships from these symbolic data sets. The Z-R relationships so obtained for CS99 and DYCOMS-II are listed below:

CS99: $Z \ [\text{mm}^6/\text{m}^3] = 8.10 \ R^{1.44} \ [\text{mm h}^{-1}]$ --------- (7)

DYCOMS-II: $Z \ [\text{mm}^6/\text{m}^3] = 17.9 \ R^{1.65} \ [\text{mm h}^{-1}]$ --------- (8)

The above relationships were found to apply to $R = [10^{-5}, 10]$ and $R = [0.001, 1]$ for equations 7 and 8, respectively. It may be noted that the coefficients in (7) and (8) are not significantly different from the medians of the corresponding parameters in Tables 2 and 3. Those values are $(a_{d3}+a_{d5})/2 = 3.9$, $(b_{d2}+b_{d3})/2 = 1.34$ for CS99 and $(a_{d10}+a_{d13})/2 = 24.9$, $(b_{d10}+b_{d13})/2 = 1.77$ for DYCOMS-II.

3.4 Extrapolation of Spectra

The concentration of larger droplets always decreases dramatically with diameter. A typical example is shown by the data points in Figure 14. Due to this fact, the particle probes with their limited sample volumes do not provide adequate samples of the larger droplets. Spectra from CS99 and from DYCOMS-II show maximum droplet sizes of up to about 300μm. To explore the impact that potential under-detection of larger droplets would have on the Z-R relationships, droplet spectra were extrapolated to droplet sizes of 500μm and 1000μm based on a best-fit line to the part of the spectrum from 30μm to the maximum detected size. An example is shown in Figure 14.

For all flight segments of DYCOMS-II, the measured one-second spectra were extrapolated to upper size limits of 500μm and 1000μm. For each second, the rain rate and reflectivity were calculated for the extrapolated spectra, and the calculated rain rate and reflectivity were used to generate a new Z-R relationship for each leg.
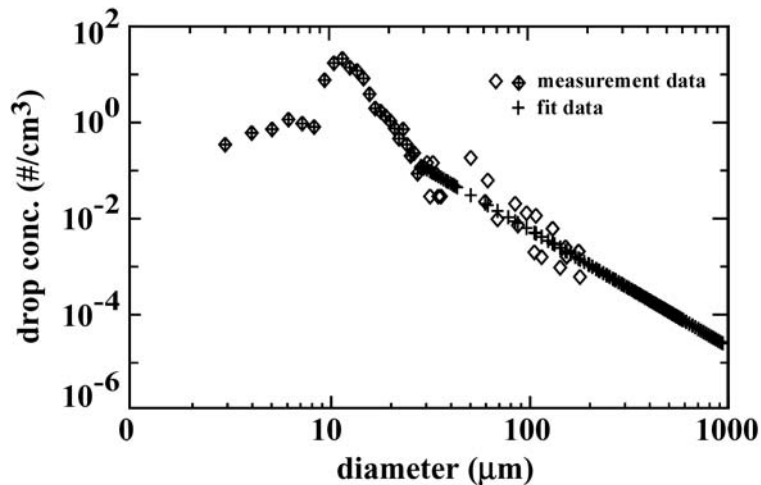
Figure 14: Example of an extrapolated spectrum (DYCOMS-II).

The histograms of Z-R parameters for spectra extrapolated to 500μm and to 1000μm are shown in Figures 15 and 16. The Z-R parameters for extrapolation to 500μm show more than 52% of the offset parameter between 20 and 30, and about 70% of the slope parameter between 1.05 and 1.35. For extrapolation to 1000μm, more than 70% of the offset parameter a, are between 60 and 70, and about 45% of the slope parameter b are between 1.07 and 1.2, however, there are extremely high a and b values for three or four legs. For extrapolation to 500μm, the correlation coefficients have an average of 0.97 with a range from 0.64 to 1.00. For extrapolation to 1000μm, the correlation coefficients have an average of 0.97, with a range from 0.55 to 1.00. The Z-R relationships so obtained, using median values of a and b for all the legs combined from DYCOMS-II are listed below:

$$Z\ [mm^6/m^3] = 23.9\ R^{1.23}\ [mm\ h^{-1}] \quad (500\mu m) \qquad \text{--------- (9)}$$

$$Z\ [mm^6/m^3] = 63.6\ R^{1.12}\ [mm\ h^{-1}] \quad (1000\mu m) \qquad \text{--------- (10)}$$

As further step, in order to reduce sensitivity to the shape of the observed one-second spectra, averaged spectra were used for the extrapolation. The observed one-second spectra were averaged over 5, 10 or 15 seconds, by averaging the number concentration per size bin of the spectra. The averaged spectra were extrapolated to droplet sizes of 500μm and 1000μm based on a best-fit line to the rest of the averaged spectrum from 30μm to the maximum detected size. For each flight segments, Z-R relationships were generated for the extrapolated averaged spectra. Table 4 gives the average, mode, and median of Z-R parameters from the extrapolated spectra. Again, the average correlation coefficients are higher than 0.95.
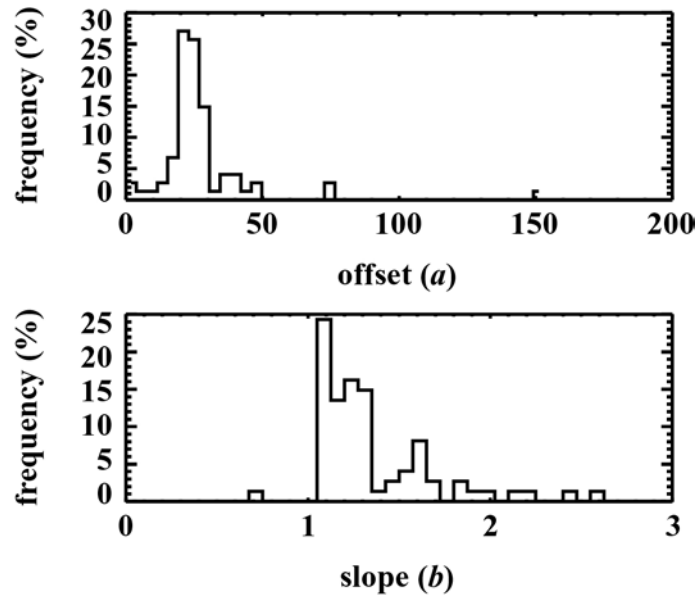
Figure 15: Histogram of Z-R parameters for extrapolation to $500\mu m$ (DYCOMS-II, 75 legs). The offset and slope are the *a* & *b* parameters in $Z = a\,R^{\,b}$.
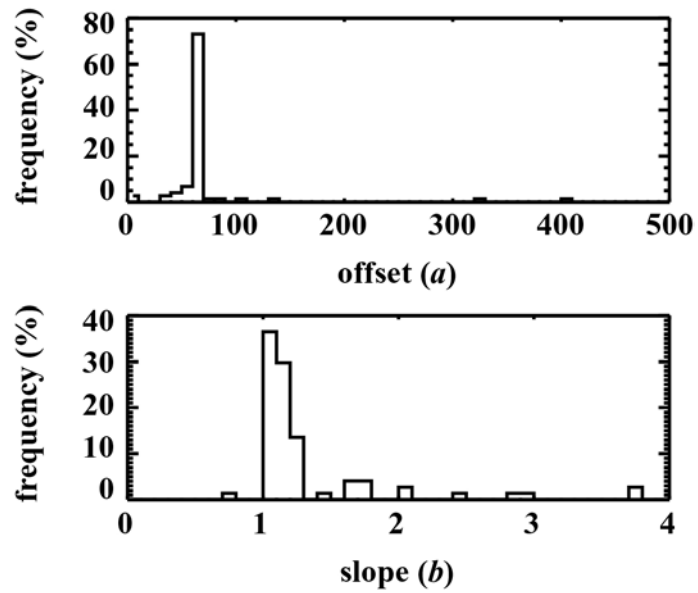
Figure 16: Histogram of Z-R parameters for extrapolation to $1000\mu m$ (DYCOMS-II, 75 legs). The offset and slope are the *a* & *b* parameters in $Z = a\,R^{\,b}$.

Table 4: Z-R parameters for extrapolated spectra of DYCOMS-II

		1-sec		5-sec		10-sec		15-sec	
		a	*b*	*a*	*b*	*a*	*b*	*a*	*b*
500μm	avg	27.8	1.36	38.6	1.39	56.1	1.40	81.7	1.46
	mode	20-25	1.1-1.2	20-25	1.1-1.2	20-25	1.1-1.2	20-25	1.1-1.2
	median	23.9	1.23	23.9	1.33	24.2	1.35	27.2	1.36
1000μm	avg	133	1.32	119	1.33	95.5	1.30	110	1.36
	mode	60-65	1.1-1.2	65-70	0.9-1.2	63-68	1.1-1.2	65-70	1.1-1.2
	median	63.6	1.12	66.9	1.14	67.1	1.18	70.1	1.20

a & *b* are constants in $Z = a R^{b}$.

As shown in Table 4, the *a* and *b* parameters tend to increase slightly with the increase of the averaging interval. It is unclear what produces this trend.

3.5 Uncertainty Analysis

If it is assumed that droplets are randomly distributed in space, and that the average rate at which particles are sampled is constant over a given interval of time, then the Poisson distribution is valid for our data. For a given size bin, the total counts per second, N, can be calculated as:

N = (sample volume per second)*(number conc. in the size bin)

The standard deviation of the mean for Poisson statistics is $\sqrt{N}$. Error bars for each size bin were constructed as $N \pm \sqrt{N}$ for each one-second spectrum. The upper and lower limits of the error bars construct two spectra (upper or lower spectra) that bracket the original data.

Since compared to observed spectra, the upper and lower spectra will either increase or decrease Z and R at the same time, the parameter β was introduced to
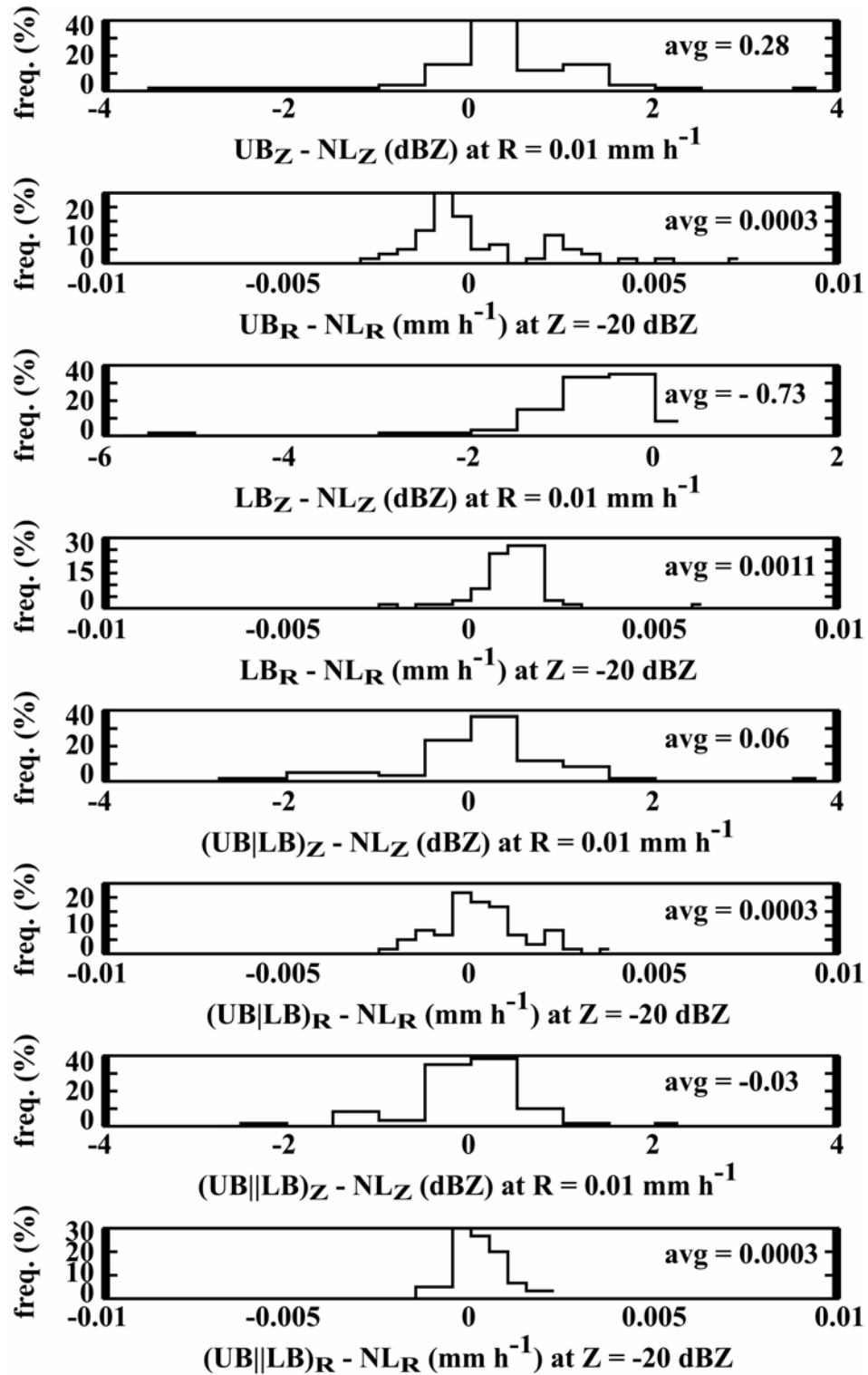
Figure 17: The uncertainties of Z-R relationship (CS99). The *freq.* at the y-axis is the occurrence frequency among 60 legs of CS99. See text for more explanation of the figure.

examine the sensitivity of the slope parameter to under or overestimation in counts:

$\beta = \dfrac{\log(Z''/Z')}{\log(R''/R')}$. Here, Z'' is the reflectivity calculated from upper spectra, Z' is the

reflectivity calculated from lower spectra, R'' is the rain rate calculated from upper

spectra, and R' is the rain rate calculated from lower spectra. The average value of β is

1.32 for CS99, fairly close to the average exponent $b = 1.58$. This indicates that effects of

counting errors are significantly reduced due to their parallel effects on R and Z.

To further quantify the impacts of possible errors, Z-R relationships were

constructed for the upper and lower bounds of the spectra in three different ways: i) Z and

R calculated from upper spectra, UB_Z and UB_R; ii) Z and R calculated from lower

spectra, LB_Z and LB_R; iii) Z and R randomly chosen to calculate from the upper or lower

spectra, $(UB|LB)_Z$, $(UB|LB)_R$, and iv) Z and R randomly given a value between the value

calculated from upper spectra and the value calculated from lower spectra, $(UB\|LB)_Z$,

$(UB\|LB)_R$. Using 0.01mm h^{-1} and -20 dBZ as typical values of R and Z for

coastal/marine stratus, Z values at R equals to 0.01mm h^{-1} and R values at Z equals to

-20 dBZ were calculated from each type of Z-R relationships. In addition, for each leg,

the Z and R values so obtained were compared with those calculated from Z-R

relationships from the measured spectra leg by leg, NL_Z and NL_R.

The histograms in Figure 17 demonstrate the results of the comparisons for CS99.

As shown, the relationship obtained from upper spectra demonstrates an average

overestimation of 0.28 dBZ at $R = 0.01$ mm h^{-1}, and an average overestimation of 0.0003

mm h^{-1} at $Z = -20$ dBZ. The Z-R relationship obtained from lower spectra demonstrates

an average underestimation of -0.73 dBZ at $R = 0.01$ mm h^{-1}, and an average

overestimation of 0.0011 mm h^{-1} at Z = –20 dBZ. The Z-R relationship for Z and R of each second randomly chosen to calculate from lower or upper spectra demonstrates an average overestimation of 0.06 dBZ at R = 0.01 mm h^{-1}, and an average overestimation of 0.0003 mm h^{-1} at Z = –20 dBZ. The Z-R relationship for Z and R randomly given a value between the one calculated from upper spectra and the one calculated from lower spectra demonstrates an average underestimation of –0.03 dBZ at R = 0.01 mm h^{-1}, and an average overestimation of 0.0003 mm h^{-1} at Z = –20 dBZ.

Cases i) and ii) represent estimates of extreme limits of the uncertainties of the Z-R relationships. In reality, the uncertainties of the Z-R relationships should be smaller than the case i) and ii), and might be close to those of the last two cases. Hence, it appears that uncertainties of the Z-R relationships due to sampling statistics are not large in comparison with other factors and do not limit the applicability of the results in comparison with other factors.

3.6 Dependence on Normalized Cloud Depth and Droplet Concentration

The Z-R relationships in this study were based on calculations from droplet size distributions (DSD), and it is well known that the DSD vary systematically in marine stratus from cloud base to cloud top. Hence, the dependence of Z-R relationships on normalized cloud depth was studied. For 7 days from CS99, Figure 18 shows Z-R slopes stratified by the level of observation in terms of the dimensionless normalized cloud depth, which is defined as 0 at cloud base and unity at cloud top. For days A, B, and D, the Z-R slope increases with the increase of normalized cloud depth; days E and H show an opposite tendency; the remaining three days show no dependence of Z-R slope on

normalized cloud depth. The exceptional tendency for days E and H might be due to data having been collected from inhomogeneous clouds that day. Study of all CS99 cases combined did not show a good correlation of cloud depth with Z-R slope, but as shown in Figure 18, there were better correlation relationships for some individual days. Day #12 was randomly chosen from DYCOMS-II, and to gain enough data for statistic purpose, each flight segment from day #12 was divided into new legs with 120 seconds in length. For this day, the Z-R slopes calculated from these new legs were found to increase with the increase of normalized cloud depth (Figure 19). Hence, using different Z-R relationships, according to cloud depth may be warranted in some cases.
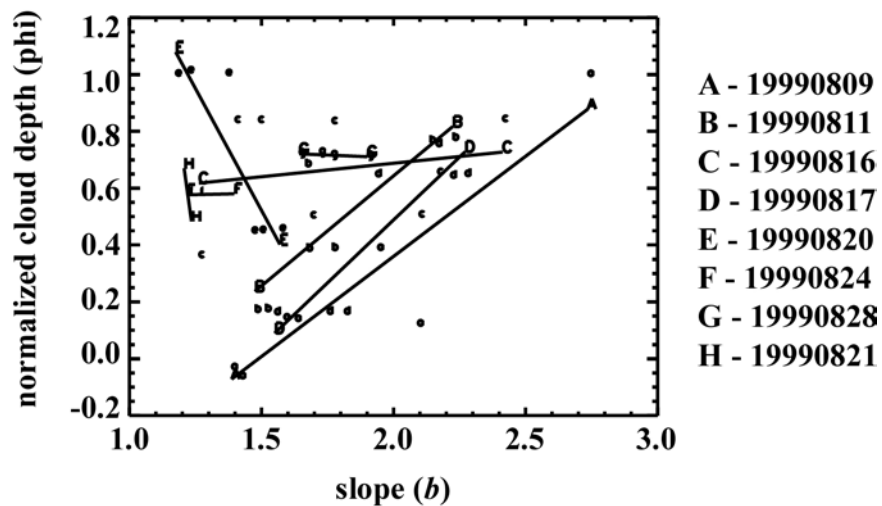
Figure 18: Normalized cloud depth vs. slope parameter by day (CS99)

It is known that for high total droplet concentrations the coalescence process proceeds slower and, therefore, the droplet spectra tend to be narrower. Hence, it may be expected that there is a dependence of the Z-R relationship on droplet concentration. Indeed, examination of the data from CS99 shows a slight increase of the Z-R slope with

28
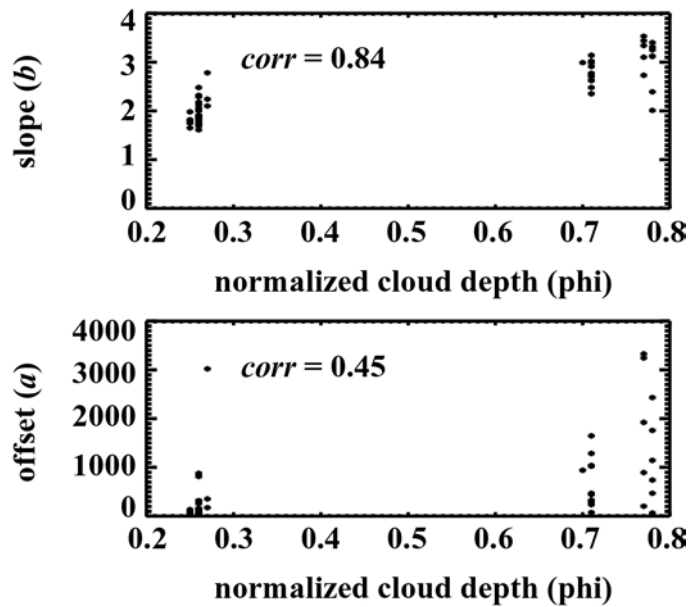
Figure 19: Histograms of Z-R parameters vs. normalized cloud depth (DYCOMS-II, 072401, day #12). *corr* is the correlation coefficients of slope and offset vs. normalized cloud depth.
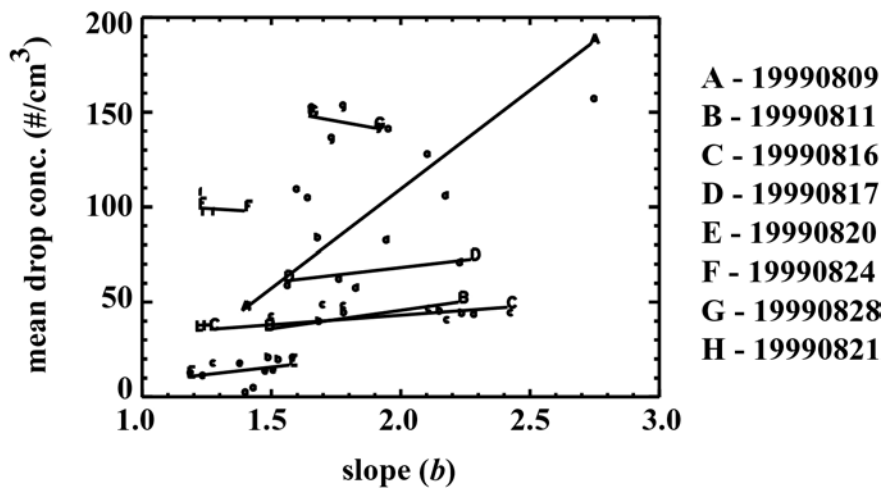
Figure 20: Mean droplet conc. vs. Z-R slope by day (CS99)

Table 5: Drizzle fraction for mass, rain rate, and reflectivity

Leg No	Dz frc for M	Dz frc for R	Dz frc for Z	phi
1	0.45	0.69	0.71	-0.04
2	0.05	0.3	0.54	0.38
3	0.39	0.7	0.74	-0.07
4	0.05	0.23	0.46	0.99
5	0.05	0.21	0.4	0.12
6	0.05	0.28	0.46	0.13
7	0.05	0.33	0.51	0.14
8	0.07	0.45	0.69	0.77
9	0.07	0.48	0.71	0.76
10	0.42	0.84	0.89	0.17
11	0.46	0.89	0.92	0.17
12	0.16	0.7	0.82	0.38
13	0.13	0.61	0.78	0.38
14	0.05	0.24	0.4	0.68
15	0.05	0.09	0.21	0.83
16	0.05	0.24	0.48	0.84
17	0.09	0.27	0.34	0.36
18	0.06	0.37	0.62	0.65
19	0.05	0.1	0.22	0.83
20	0.05	0.08	0.15	0.83
21	0.05	0.25	0.46	0.5
22	0.05	0.19	0.36	0.5
23	0.05	0.18	0.39	0.64
24	0.05	0.08	0.2	0.75
25	0.12	0.73	0.89	0.16
26	0.14	0.78	0.91	0.16
27	0.15	0.78	0.9	0.16
28	0.06	0.48	0.78	0.64
29	0.05	0.28	0.53	0.64
30	0.1	0.25	0.34	1
31	0.13	0.34	0.44	1.01
32	0.24	0.64	0.74	0.44
33	0.19	0.66	0.78	0.45
34	0.12	0.38	0.51	1
35	0.21	0.59	0.7	0.45
36	0.07	0.08	0.08	0.67
37	0.14	0.15	0.16	0.48
38	0.05	0.06	0.08	0.57
39	0.05	0.06	0.08	0.58
40	0.05	0.06	0.08	0.57
41	0.05	0.06	0.09	0.58
50	0.05	0.14	0.29	0.71
51	0.05	0.15	0.31	0.71
52	0.05	0.12	0.24	0.72
53	0.05	0.09	0.18	0.72
avg	0.11	0.35	0.48	0.54
min	0.05	0.06	0.08	-0.07
max	0.46	0.89	0.92	1.01

increase of droplet concentration for most days studied as shown in Figure 20. This factor deserves further study.

3.7 Drizzle

In order to gain an appreciation of the importance of drizzle in the clouds examined, the moments of the 1-second droplet spectra were separated into two parts: thepart due to cloud droplets (D<50μm) and the part due to drizzle. For CS99, 45 flight segments, which have the normalized cloud depth information available, were examined and the averaged fractions for each leg were calculated. The detailed information is presented in Table 5 along with the normalized cloud depth for each leg. For those legs of CS99, the drizzle fraction of mass has an average of 11%, and ranges from 5% to 46%; the drizzle fraction of rain rate has an average of 35%, and ranges from 6% to 89%; the drizzle fraction of reflectivity has an average of 48%, and ranges from 8% to 92%. The drizzle contribution is greatest to Z and least to M, as expected for higher moments of the DSD. As shown in Table 5, drizzle existed in each level examined in cloud or right under cloud base, and higher drizzle fraction was found at cloud base or close to cloud base.

4. Summary

Drop size distribution (DSD) measured by airborne probes in CS99 and DYCOMS-II projects were used to investigate the relationship between rain rate (R) and reflectivity (Z) for marine stratus. Z-R relationships were determined for each flight segment chosen and also for data combined by day and by project.

31

Correlation coefficients of log(Z) and log(R) for individual legs have an average of 0.96 for CS99 and 0.93 for DYCOMS-II, providing support for the validity of the derived power-law equations of the form $Z = a\, R^{\,b}$. For CS99, the offset parameter a_{si} (i = 1-60) varies from 1.2 to 115 with about 28% of the values falling between 1.2 and 5; the slope parameter b_{si} (i = 1-60) varies from 1.1 to 2.8, with about 17% of the values between 1.2 and 1.3 and about 73% between 1.2 and 1.8. DYCOMS-II data exhibit larger variability in Z-R parameters: the offset a_{si} (i = 61-135) in Figure 6 varies from 1.4 to around 1000, with 26% of the values less than 25 and about 58% less than 75; the slope b_{si} (i = 61-135) range from 1.1 to 3.8 with 13% of the values between 1.6 and 1.7 and 37% between 1.6 and 2.0.

A Z-R relationship for each flight day was obtained by combining all the data of that day. For CS99 project, the daily values of a_{dj} (j = 1-8) vary from 0.8 to 41.1 and from 1.14 to 2.01 for b_{dj} (j = 1-8). Again, greater variation was found in daily Z-R parameters for DYCOMS-II. For the six days studied, the day-to-day variation is 2.5 to 166.8 for a_{dj} (j = 9-14), and 1.37 to 2.01 for b_{dj} (j = 9-14).

The Z-R relationships for the projects were obtained using synthetic data points generated from the Z-R equations of all individual flight segments within their ranges of validity. This procedure yielded the following equations:

CS99: $\qquad\qquad\qquad\quad Z\,[\text{mm}^6/\text{m}^3] = 8.10\, R^{\,1.44}\,[\text{mm h}^{-1}]$ $\qquad$ --------- (7)

DYCOMS-II: $\qquad\qquad\quad Z\,[\text{mm}^6/\text{m}^3] = 17.9\, R^{\,1.65}\,[\text{mm h}^{-1}]$ $\qquad$ --------- (8)

The range of validity is about $R = [10^{-5}, 10]$ and $R = [0.001, 1]$ for equations 7 and 8, respectively.

To explore the impact that potential under-detection of larger droplets might have on Z-R relationships, extrapolations were made of the measured spectra to 500μm and 1000μm based on a best-fit line to the part of the spectrum with drop size bigger than 30μm. For the DYCOMS-II data, this procedure yielded the following Z-R relationships:

$$Z \ [mm^6/m^3] = 23.9 \ R^{1.23} \ [mm \ h^{-1}] \quad (500μm) \qquad --------- (9)$$

$$Z \ [mm^6/m^3] = 63.6 \ R^{1.12} \ [mm \ h^{-1}] \quad (1000μm) \qquad --------(10)$$

Equations 7-10 are plotted in Figure 21. It may be noted that the differences between the relationships for the two data sets obtained in stratocumulus over the eastern Pacific Ocean are in relatively close agreement. The Z-R relationship

$$Z \ [mm^6/m^3] = 12.0 \ R^{1.55} \ [mm \ h^{-1}] \qquad --------- (11)$$

is a reasonably good fit to the equations derived for the two projects separately. Thus, as a general result for marine stratus over the eastern Pacific, the use of the equation 11 is suggested. The range of validity for equation 11 is the overlap range of validity for equations 7 and 8, i.e. 0.001 to 1 mm h^{-1} in R, or about –35 to 10 dBZ in Z.

The Z-R relationships for extrapolated spectra show comparatively larger differences for low R values; as could be expected, it is for small drizzle rates that the inclusion of large drops makes the largest difference. Comparison of the lines in Figure 21 shows that under-estimation of the concentrations of larger drops tends to produce Z-R relationship which may over-estimate the rain rate for given Z. But the applicability of the Z-R relationship obtained from extrapolation compared to those generated from observations need to be examined further.

The magnitudes of the uncertainties of the derived Z-R relationships were estimated based on Poisson statistics for typical Z and R values. In extreme cases, the
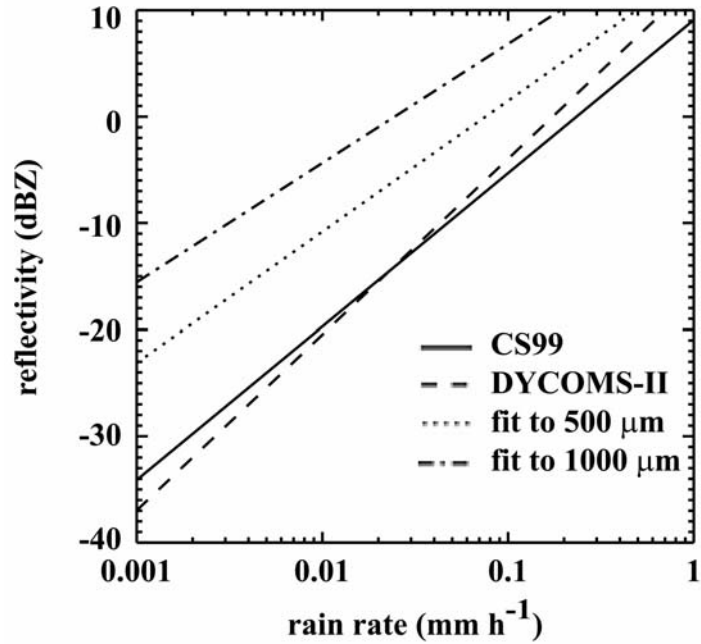
Figure 21: Comparison of Z-R relationships obtained

error from sampling may cause an overestimate of 0.28 dBZ for Z and 0.0011 mm h^{-1} for R. Simulations of random sample errors for each second of data indicated an average uncertainty of less than 0.03 dBZ for Z and an average overestimate of 0.0003 mm h^{-1} for R. Hence, it appears that uncertainties of the Z-R relationships due to sampling statistics are not large in comparison with other factors and do not limit the applicability of the results.

The dependence of the Z-R relationship on normalized cloud depth and droplet concentration was examined for selected days. It was found that the Z-R slope increases with normalized cloud depth and mean drop concentration. Hence, using different Z-R relationships, according to normalized cloud depth and mean drop concentration may be warranted in some cases.

The relative contributions of drizzle (D>50μm) to total mass, rain rate, and reflectivity were investigated for the CS99 project. The average drizzle fraction is 11% for mass, 35% for rain rate, and 48% for reflectivity. Hence, the drizzle contribution is greatest to Z and least to M, as expected for higher moments of the DSD.

Further work could include: (1) investigating more covariants that influence the Z-R relationships, (2) comparing the Z-R relationships obtained from this study with Z_{obs}-R relationships for CS99 and DYCOMS-II, where Zobs is measured reflectivity, and (3) evaluating the applicability of the Z-R relationships to other marine stratus cases.

BIBILIOGLOGHY

Battan, L. J., 1973: Radar observation of the atmosphere. University of Chicago Press, Chicago, IL, 90-92pp.

Brandes, E. A., J. Vivekanandan, and J. W. Wilson, 1999: Notes and correspondence: A comparison of radar reflectivity estimates of rainfall from collocated radars. *J. Atmos. Sci.*, 16, 1264-1272.

Caton, P. G. F, 1964: A study of raindrop size distributions in the free atmosphere. *Proc. Eleventh Wea. Radar Conf.*, Boston: Amer. Meteor. Soc, 136-141pp.

Frisch, A. S., G. Feingold, C. W. Fairall, T. Uttal, and J. B. Snider, 1998: On cloud radar and microwave radiometer measurements of stratus cloud liquid water profiles. *J. Geophy. Res.*, 103, 23195-23197.

Gunn, R., and G. D. Kinzer, 1949: The terminal velocity of fall for water droplets in stagnant air. *J. Appl. Meteor.* 21, 252-256.

Robert A. Houze, Jr., 1993: Cloud dynamics. Academic Press, Inc, San Diego, California, 137pp

Martin, G. M., D. W. Johnson, and A. Spice, 1994: The measurement and parameterization of effective radius of droplets in warm stratocumulus clouds. *J. Atmos. And Ocean Tech.*, 51, 1823-1842.

Nicholls, S., 1984: The dynamics of stratocumulus: Aircraft observations and comparisons with a mixed layer model. *Quart. J. Roy. Meteor. Soc.*, 112, 431-460

Randall, D. A., J. A. Coakley Jr., C. W. Fairall, R. A. Kropfli, and D. H. Lenschow, 1984: Outlook for research on subtropical marine stratiform clouds. *Bull. Amer. Meteor. Soc.*, 65, 1290-1310.

Rogers, R. R. and M. K. Yau, 1989: A short course in cloud physics. McGill University, Canada, 125-126pp

Seliga, T. A., K. Aydin, and H. Direskeneli, 1986: Disdrometer measurements during intense rainfall event in central Illinois: Implications for differential reflectivity radar observations. *J. Cli. and Appl. Meteor.*, 25, 835-84

Vali, G., R. D. Kelly, J. French, S. Haimov, and D. Leon, 1998, Finescale Structure and Microphysics of Coastal Stratus. *J. Atmos. Sci.*, 55, 3540-3564

Short flight segments of CS99

leg No (i)	date	start time	end time	duration	Z-R parameters		
	yymmdd	hhmmss	hhmmss	seconds	a_{si}	b_{si}	$corr_{si}$
1	080999	164636	164836	120	18.30	1.39	0.98
2	080999	173102	173922	500	76.47	1.94	0.87
3	080999	174603	175033	270	22.61	1.42	0.97
4	080999	180500	180907	247	653.75	2.74	0.91
5	080999	185323	185523	120	44.25	2.09	0.87
6	080999	193519	193938	259	20.37	1.63	0.91
7	080999	194038	194433	235	18.28	1.59	0.83
8	081199	144701	145437	456	54.76	2.22	0.95
9	081199	145528	150752	744	47.03	2.14	0.92
10	081199	155042	155545	303	15.27	1.48	0.97
11	081199	155627	160140	313	17.51	1.51	0.97
12	081199	160254	160745	291	26.60	1.77	0.97
13	081199	160853	161348	295	19.93	1.67	0.96
14	081199	164521	164808	167	13.13	1.67	0.98
15	081699	164223	164423	120	4.02	1.49	0.76
16	081699	164544	165134	350	193.54	2.41	0.94
17	081699	165453	165710	137	3.55	1.26	0.95
18	081699	170040	170343	223	118.01	2.17	0.96
19	081699	172645	173017	212	11.51	1.77	0.89
20	081699	173221	173823	362	2.53	1.40	0.93
21	081699	173903	174502	359	112.84	2.10	0.90
22	081699	174543	175138	355	15.70	1.69	0.92
23	081799	142934	143416	282	22.12	1.93	0.90
24	081799	143511	143722	131	48.30	2.16	0.75
25	081799	150511	150811	180	26.32	1.75	0.96
26	081799	150913	151411	298	29.48	1.81	0.97
27	081799	151459	151815	196	15.09	1.55	0.97
28	081799	152006	152342	216	69.12	2.22	0.93
29	081799	164823	165023	120	64.04	2.27	0.94
30	082099	153240	153647	247	1.42	1.18	0.98
31	082099	153729	154221	292	1.89	1.22	0.99
32	082099	160044	160633	349	7.13	1.46	0.97

33	082099	160846	161232	226	11.00	1.57	0.98
34	082099	163239	163647	248	3.05	1.37	0.97
35	082099	163737	164254	317	7.36	1.50	0.96
36	082199	150222	150623	241	1.19	1.21	0.99
37	082199	152833	153420	347	1.36	1.24	1.00
38	082499	173639	174143	304	1.01	1.23	0.91
39	082499	174217	174825	368	2.20	1.40	0.92
40	082499	180241	180538	177	1.26	1.27	0.90
41	082499	180719	181316	357	1.01	1.22	0.97
42	082499	11946	12217	151	1.24	1.13	1.00
43	082499	14409	14646	157	4.59	1.50	0.97
44	082499	14802	15035	153	3.69	1.44	0.97
45	082499	15257	15556	179	2.21	1.28	0.99
46	082599	160928	161310	222	12.97	1.55	0.97
47	082599	162810	163010	120	5.36	1.26	0.94
48	082599	164047	164341	174	2.47	1.26	0.99
49	082599	164443	164704	141	3.12	1.32	0.97
50	082999	175147	175740	353	12.54	1.77	0.95
51	082999	175825	180359	334	21.53	1.90	0.86
52	082999	182811	183331	320	10.06	1.72	0.91
53	082999	183414	184005	351	6.78	1.64	0.84
54	082999	175239	175444	125	37.77	1.58	0.95
55	082999	175649	175849	120	40.16	1.64	0.97
56	082999	180118	180323	125	68.46	1.65	0.95
57	082999	180528	180824	176	96.41	1.92	0.92
58	082999	182323	182641	198	37.56	1.49	0.98
59	082999	184227	184517	170	25.47	1.74	0.97
60	082999	191349	191552	123	41.15	1.39	0.97

APPENDIX B

Short flight segments of DYCOMS-II

leg No (i)	date	start time	end time	duration	Z-R relationship		
	yymmdd	hhmmss	hhmmss	seconds	a_{si}	b_{si}	$corr_{si}$
61	071101	110800	111259	300	0.84	1.16	0.93
62	071101	111300	111759	300	1.44	1.34	0.96
63	071101	111800	112259	300	23.86	2.57	0.91
64	071101	112300	112759	300	24.87	2.58	0.93
65	071101	112800	113259	300	15.35	2.39	0.94
66	071101	113300	113759	300	4.34	1.78	0.78
67	071101	113800	114000	121	1.42	1.37	0.88
68	071101	114130	114629	300	3.04	1.65	0.86
69	071101	114630	115129	300	15.47	2.41	0.94
70	071101	115130	115629	300	36.58	2.74	0.91
71	071101	115630	120129	300	35.84	2.82	0.91
72	071101	120130	120629	300	1.38	1.33	0.95
73	071101	120630	120837	128	1.13	1.28	0.95
74	071301	100700	101259	300	207.9	2.28	0.87
75	071301	101300	101759	300	502.54	2.57	0.9
76	071301	101800	102259	300	127.16	2.15	0.92
77	071301	102300	102759	300	319.19	2.31	0.93
78	071301	102800	103300	301	282.33	2.35	0.86
79	071301	82648	83247	360	57.5	1.84	0.94
80	071301	83248	84001	434	55.37	1.82	0.96
81	071301	103643	104155	313	163.57	2.11	0.94
82	071301	104810	105309	300	177.14	2.18	0.9
83	071301	105310	105955	406	535.91	2.48	0.92
84	071301	124100	124842	463	69.98	1.85	0.89
85	071701	83822	84525	424	305.57	2.11	0.93
86	071701	90807	91306	300	171.87	2.03	0.97
87	071701	91307	91806	300	149.33	2.01	0.98
88	071701	91807	92306	300	1772.81	2.44	0.98
89	071701	92307	92600	174	1168.63	2.32	0.98
90	072401	85344	85843	300	55.69	1.79	0.95
91	072401	85844	90343	300	102.45	1.94	0.96
92	072401	90344	90843	300	343.24	2.29	0.97

93	072401	90844	91343	300	37.06	1.75	0.96
94	072401	91344	91843	300	35.4	1.62	0.95
95	072401	91844	92100	137	56.08	1.75	0.95
96	072401	92313	93119	487	47.74	1.73	0.97
97	072401	93410	93909	300	162.73	2	0.96
98	072401	93910	94346	277	376.24	2.18	0.96
99	072401	94347	94846	300	120.03	1.92	0.96
100	072401	94847	95317	271	132.25	1.98	0.98
101	072401	113858	114357	300	2143.99	3.37	0.91
102	072401	114358	114857	300	2418.2	3.42	0.93
103	072401	114858	115357	300	1898.72	3.42	0.9
104	072401	115358	115820	263	280.83	2.84	0.87
105	072401	115854	120353	300	39.07	2.12	0.92
106	072401	120354	120918	325	10141	3.79	0.93
107	072401	121144	121643	300	636.11	2.86	0.95
108	072401	121644	122143	300	58.98	2.08	0.87
109	072401	122144	122643	300	257.07	2.61	0.93
110	072401	122644	123143	300	951.99	2.95	0.91
111	072401	123144	123643	300	959.75	2.98	0.94
112	072401	123644	124100	257	2562.1	3.33	0.92
113	072501	221800	222259	300	27.92	1.78	0.96
114	072501	222300	222759	300	15.57	1.62	0.96
115	072501	222800	223431	392	9.22	1.44	0.94
116	072501	223453	223952	300	15.13	1.64	0.97
117	072501	223953	224600	368	19.56	1.7	0.96
118	072501	224800	225259	300	132.97	2.21	0.9
119	072501	225300	225759	300	40.17	1.99	0.93
120	072501	225800	230351	352	22.43	1.82	0.93
121	072501	230630	231129	300	15.67	1.66	0.94
122	072501	264400	264859	300	0.65	1.16	0.99
123	072501	264900	265359	300	1.23	1.3	0.99
124	072501	265400	265859	300	204.16	2.59	0.94
125	072501	265900	270359	300	299.62	2.72	0.9
126	072501	270400	270859	300	836.05	2.82	0.96
127	072501	270900	271345	286	0.69	1.18	0.99
128	072501	272500	273300	481	68.03	2.33	0.88
129	072701	213300	213803	304	20.39	1.86	0.95
130	072701	214308	214548	161	16.94	1.78	0.84
131	072701	215006	215615	370	35.73	1.92	0.96

132	072701	215821	220404	344	30.05	1.89	0.94
133	072701	222100	222533	274	28.59	1.74	0.98
134	072701	222835	223434	360	23.02	1.69	0.96
135	072701	223642	224239	358	25.19	1.71	0.97